Powder Technology 227 (2012) 35–42

Contents lists available at SciVerse ScienceDirect

Powder Technology

journal homepage: www.elsevier.com/locate/powtec

# Shape control mechanism of cuprous oxide nanoparticles in aqueous colloidal solutions

Yakui Bai [1], Tengfei Yang [1], Qing Gu, Guoan Cheng, Ruiting Zheng *

*College of Nuclear Science and Technology, Beijing Normal University, Beijing 100875, China*

ARTICLE INFO

*Article history:*
Received 29 October 2011
Received in revised form 28 January 2012
Accepted 4 February 2012
Available online 11 February 2012

*Keywords:*
Cuprous oxide
Self-assembly
Crystalline
Sol–gel

ABSTRACT

Cuprous oxide ($Cu_2O$) nanoparticles with various particle shapes were synthesized via colloidal chemistry approach. Using ascorbic acid as a reducing agent and polyvinylpyrrolidone (PVP) as a surfactant, cuprous oxide monocrystalline nanoparticles with various sizes have been successfully synthesized by reaction of bivalent copper in aqueous solution. The samples were characterized by XRD, SEM and UVs spectroscopy. The results indicate the shape of as-prepared cuprous oxide nanoparticles has close relationship with thermodynamic conditions, kinetic conditions and stirring rate. Self-assembly mechanism of cubic cuprous oxide monocrystalline nanoparticles has also been investigated.



## 1. Introduction

Cuprous oxide and cupric oxide have been investigated for decades due to their unique semiconductor and optical properties [1]. As a P-type semiconductor material, the theoretical direct band gap of cuprous oxide is about 2.2 eV [2]. In aspect of photoluminescence, cuprous oxide has a very long excited lifetime (about 10 μs) [3,4]. Solid-state cuprous oxide also shows a light-emitting coherence character [5]. Cuprous oxide has potential applications in solar cells [6], nano-magnetic devices [7], chemical industry [8], biosensors [9] and so on. It is also reported that cuprous oxide microspheres have been used as cathode material of lithium battery and photocatalyst in the visible light which led to photochemical decomposition of $H_2O$ and generation of $O_2$ and $H_2$ [10].

Controlled fabrication of semiconductor nanomaterial is of special interest in the field of nanoscience and nanotechnology [11], because a structure–function relationship is the underlying motive for discovering novel nanoscale structures. The preparation of different forms of cuprous oxide particles are mainly prepared by liquid chemistry method.

In the past few years, numerous $Cu_2O$ nanostructures, including nanosheets [12], nanocubes [13], octahedra [14], spherical particles [15], nanoboxes [16], and nanowires [17,18] have been synthesized. The geometry shape control and detailed crystal structure analysis of cuprous oxides have been performed on these $Cu_2O$ nanocrystals. However, the growth mechanism, which is important for the controlled synthesis of $Cu_2O$ nanocrystals, still needs a detailed investigation.

Among the above methods for the preparation of $Cu_2O$ nanoparticles, flammable or corrosive reducing agent such as titanium tetrachloride [12] and hydrazine [15,17] was used. Other wet-chemical synthesis methods adopt toxic organic reactant such as ethylene glycol [16]. Ethylene glycol is easy oxidized in air to glycolic acid which is corrosive, in turn, oxidized to oxalic acid, which is toxic. Such toxic organic reactant was not suitable in industrial production because of toxicity and relatively high material cost. Additional assistant reducing agent such as sodium tartrate was required in certain method [14]. High temperature (over 100 degrees) heating step (oil bath) was required in some synthesis process [16]. On the other hand, significant energy was demanded for high temperature reaction environment [16] and electrodeposition [18] in case of large-scale synthesis and there are many factors of insecurity in procedure. Templates, cetyl trimethyl ammonium bromide (CTAB) [17] and anodic aluminum oxide (AAO) [18] have been successfully employed to prepare $Cu_2O$ nanocrystals with specific morphologies, such as nano-whiskers and nanowires. A simple and green synthetic route for nanosized $Cu_2O$ nanostructures with single-crystalline is sorely needed. The single-crystalline $Cu_2O$ with varied nanostructures are produced by a one-pot, solution-phase and template free method.

In this paper, we adopt a colloidal chemistry approach for the syntheses of monodispersed $Cu_2O$ nanocubes, truncated nanocubes, cuboctahedra, nanosphere, and octahedra by adjusting experimental conditions, detecting the influence of experimental conditions on the morphology evolution of $Cu_2O$ nanocrystals. Based on our observation and analysis, the growth mechanism of $Cu_2O$ nanocrystals is elucidated.

* Corresponding author. Tel./fax: +86 10 62205403.
*E-mail address:* rtzheng@bnu.edu.cn (R. Zheng).
[1] The first two authors have same contributions to this paper.

0032-5910/$ – see front matter © 2012 Elsevier B.V. All rights reserved.
doi:10.1016/j.powtec.2012.02.008

## 2. Experimental

### 2.1. Chemicals

Copper acetate ($Cu(CH_3COO)_2•H_2O$, AR) and ascorbic acid ($C_6H_8O_6$, AR) were purchased from Shantou Xilong Chemical Plant. Polyvinylpyrrolidone (PVP) (K30, molecular weight of 10,000), sodium hydroxide (NaOH, AR) and deionized water were purchased from Beijing Chemical Reagents Inc. All chemicals are used without further purification.

### 2.2. Synthesis of $Cu_2O$ nanoparticles

$Cu_2O$ nanoparticles were prepared by the reaction of $Cu(CH_3COO)_2$ with $C_6H_8O_6$ at different temperatures. Typically, 0.25 mmol (0.05 g) of cupric acetate and 0.005 mmol (in repeating unit) of polyvinylpyrrolidone (PVP) were dissolved in 100 ml deionized water and formed a blue aqueous solution, and 5 mmol (0.2 g) of sodium hydroxide was dissolved in 20 ml of deionized water too. Then the as-prepared sodium hydroxide solution (0.25 mol/l) was added dropwise into the cupric acetate solution (2.5 mmol/L) at room temperature, under vigorous stirring. The solution turned to be a blue suspension. 0.75 mmol (0.132 g) of ascorbic acid was dissolved in 15 ml of deionized water and a transparent solution formed, then the ascorbic acid aqueous solution (0.05 mol/l) was added into the above blue suspension at the speed of 3 drops per second under vigorous stirring. The color of the suspension changes from blue to green; finally, a reddish suspension was obtained after 30 min of reaction. The as-prepared products were centrifuged from the solution at 4000 rpm for 15 min by a Biofuges Stratos centrifuge (Thermo Fisher Scientific). The derived products were washed with deionized water three times and dried in air for characterization. By changing the molar ratio of ascorbic acid to cupric acetate, the amount of surfactant, the stirring rate and the reaction temperature, $Cu_2O$ nanoparticles exhibiting different structures were obtained.

Six series of experiments were first carried out to reveal the effects of experimental conditions on the morphology of $Cu_2O$ nanoparticles. All the experimental conditions and the morphologies of cuprous oxide are summarized in Table 1. Table 1 lists the average size of $Cu_2O$ nanoparticle in every experimental condition with only one parameter changed. The parameters changed in each experimental condition are amount of copper salt, amount of surfactant, temperature, amount of ascorbic acid, stirring rate, and amount of NaOH, respectively.

### 2.3. Characterization

Crystal structure of the $Cu_2O$ nanoparticles was identified by a powder X-ray diffractometer (XRD) (PANalytical X'Pert), employing Cu-Kα radiation ($\lambda = 1.5418$ Å) at 50 kV and 200 mA. The morphology of the $Cu_2O$ nanoparticle was observed by a field emission scanning electron microscopy (SEM) (Hitachi S-4800, Japan) at 5 kV. Particle size was analyzed by Image-Pro software. Crystal structure and growth orientation of the $Cu_2O$ nanoparticles were characterized by a high resolution transmission electron microscopy HRTEM (Philips FEI TECNAI F30) at 200 kV. The ultraviolet and visible light (UV–vis) absorption spectrum was recorded by a Shimadzu UV-365 PC spectrophotometer.

In order to measure the average size of product accurately, we use image analysis software (Image Pro-Plus 6) to analyze the SEM images. If the shape of product was spherical, the size means diameter. If the shape of product was polyhedron, the size denotes edge length of equal volume cube. If the shape of product was cube or truncated cube, the size was edge length. If the shape of product was octahedron, the average size was referring to edge length of equal volume cube.

## 3. Results

As described in Fig. 1, cupric acetate could be dissolved in water and forms a uniform ionic solution. When the NaOH is added in the solution, the $Cu^{2+}$ react with $OH^-$ and forms insoluble $Cu(OH)_2$ nanowires, as Fig. 1A shows. While $Cu(OH)_2$ suspension reacts with ascorbic acid, $Cu(OH)_2$ will be dissolved and reduced into $Cu_2O$

**Table 1**
Summary of the experimental conditions and as-prepared products.

| Sample | Cu(II) (mmol) | Surfactant (mmol) | Temperature (°C) | Reducer (ml) | Stirring rate (r/s) | NaOH (g) | Average size (nm) | Morphologies |
|---|---|---|---|---|---|---|---|---|
| $A_1$ | 1 | 0.005 | 20 | 15 | 5 | 0.2 | 1700 | Sphericity |
| $A_2$ | 0.5 | 0.005 | 20 | 15 | 5 | 0.2 | 800 | Sphericity |
| $A_3$ | 0.25 | 0.005 | 20 | 15 | 5 | 0.2 | 200 | Polyhedron |
| $A_4$ | 0.15 | 0.005 | 20 | 15 | 5 | 0.2 | 150 | Polyhedron |
| $A_5$ | 0.1 | 0.005 | 20 | 15 | 5 | 0.2 | 100 | Polyhedron |
| $A_6$ | 0.05 | 0.005 | 20 | 15 | 5 | 0.2 | 100 | Sphericity |
| $B_1$ | 0.25 | 0.5 | 20 | 15 | 5 | 0.2 | 700 | Cube |
| $B_2$ | 0.25 | 0.2 | 20 | 15 | 5 | 0.2 | 500 | Polyhedron |
| $B_3$ | 0.25 | 0.1 | 20 | 15 | 5 | 0.2 | 300 | Polyhedron |
| $B_4$ | 0.25 | 0.005 | 20 | 15 | 5 | 0.2 | 200 | Polyhedron |
| $B_5$ | 0.25 | 0.002 | 20 | 15 | 5 | 0.2 | 100 | Polyhedron |
| $B_6$ | 0.25 | 0.001 | 20 | 15 | 5 | 0.2 | 100 | Polyhedron |
| $C_1$ | 0.25 | 0.005 | 90 | 15 | 5 | 0.2 | 150 | Cube |
| $C_2$ | 0.25 | 0.005 | 50 | 15 | 5 | 0.2 | 500 | Cube |
| $C_3$ | 0.25 | 0.005 | 40 | 15 | 5 | 0.2 | 400 | Cube |
| $C_4$ | 0.25 | 0.005 | 30 | 15 | 5 | 0.2 | 150 | Truncated cube |
| $C_5$ | 0.25 | 0.005 | 20 | 15 | 5 | 0.2 | 150 | Truncated cube |
| $C_6$ | 0.25 | 0.005 | 4 | 15 | 5 | 0.2 | 300 | Truncated cube |
| $D_1$ | 0.25 | 0.005 | 20 | 20 | 5 | 0.2 | 250 | Octahedron |
| $D_2$ | 0.25 | 0.005 | 20 | 15 | 5 | 0.2 | 100 | Truncated cube |
| $D_3$ | 0.25 | 0.005 | 20 | 10 | 5 | 0.2 | N/A | Spicule |
| $D_4$ | 0.25 | 0.005 | 20 | 5 | 5 | 0.2 | N/A | Spicule |
| $E_1$ | 0.25 | 0.005 | 20 | 15 | 5.5 | 0.2 | 150 | Sphericity |
| $E_2$ | 0.25 | 0.005 | 20 | 15 | 5 | 0.2 | 150 | Polyhedron |
| $E_3$ | 0.25 | 0.005 | 20 | 15 | 4.5 | 0.2 | 250 | Truncated cube |
| $E_4$ | 0.25 | 0.005 | 20 | 15 | 4 | 0.2 | 750 | Cube |
| $F_1$ | 0.25 | 0.005 | 20 | 15 | 5 | 0.5 | 250 | Truncated cube |
| $F_2$ | 0.25 | 0.005 | 20 | 15 | 5 | 0.1 | 200 | Polyhedron |
| $F_3$ | 0.25 | 0.005 | 20 | 15 | 5 | 0.05 | 150 | Polyhedron |
| $F_4$ | 0.25 | 0.005 | 20 | 15 | 5 | 0.01 | 500 | Dandelion |

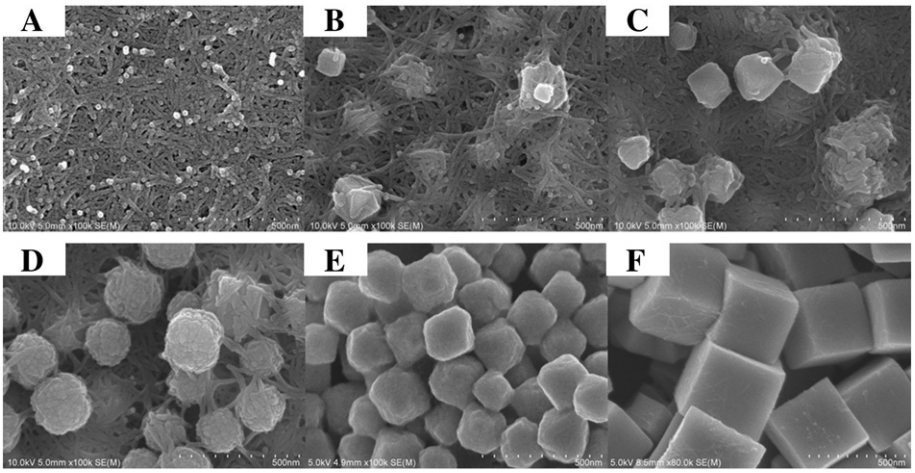


**Fig. 1.** SEM images of intermediate product at different reaction times. (A) 30 s, (B) 60 s, (C)120 s, (D) 300 s, (E) 600 s, and (F)1800 s.

nanoparticles. When subsequent $Cu_2O$ monomers precipitate from the solution, they tend to aggregate on the existing $Cu_2O$ seeds and grow up (Fig. 1B–D). After 300 s of reaction, all the $Cu(OH)_2$ nanowires transform into $Cu_2O$ nanoparticles. Ripening and surface reconstruction processes take place in the next 20 min to form the final nanocrystal structures with distinct shapes (Fig. 1E–F).

Fig. 2 illustrates the microstructures of typical $Cu_2O$ nanocubes synthesized using our approach. Fig. 2A shows a SEM image of the samples. The nanoparticles exhibit typical cubic morphology with a mean edge length of 255 nm and a standard deviation of 35 nm. It could be observed that the corners of some nanocubes were truncated. Fig. 2B shows the TEM image of a $Cu_2O$ nanocube on the surface of a TEM grid. The inset shows the selected area electron diffraction (SAED) patterns obtained by directing the electron beam perpendicular to the square faces of the cube; The square symmetry of this pattern indicates that each $Cu_2O$ nanocube was a single crystal bounded mainly by {100} facets. Fig. 2C is the XRD pattern of a reaction product in the 2θ range of 10–80°. The XRD pattern could be distinctly indexed to a cubic phase with lattice constants a = 4.270 Å for $Cu_2O$ ((ICDD No. 99-0041). No peaks from other impurities can be detected in the XRD pattern, indicating that phase-pure cuprous oxide can be synthesized in the solution phase by reduction of copper acetate. It is worth noting that the ratio between the intensities of the (111) and (200) diffraction peaks was lower than the conventional value (1.381 versus 3.105), indicating that our nanocubes were abundant in {100} facets. Truncated corner of $Cu_2O$ nanocubes corresponds to {111} facets. UV–vis absorption spectra of cuprous oxide nanoparticles were demonstrated in Fig. 2D. The characteristic absorption peak is due to plasma resonance excitation of copper atoms on the surface of nanocubes [19,20]. The absorption peak lies around 484 nm. The calculated direct band gap of our cuprous oxide is 2.56 eV, slightly higher than the theoretical direct band gap of 2.2 eV.

The morphology and the average size of the nanoparticles could be tuned by adjusting the reaction conditions such as reaction temperature,

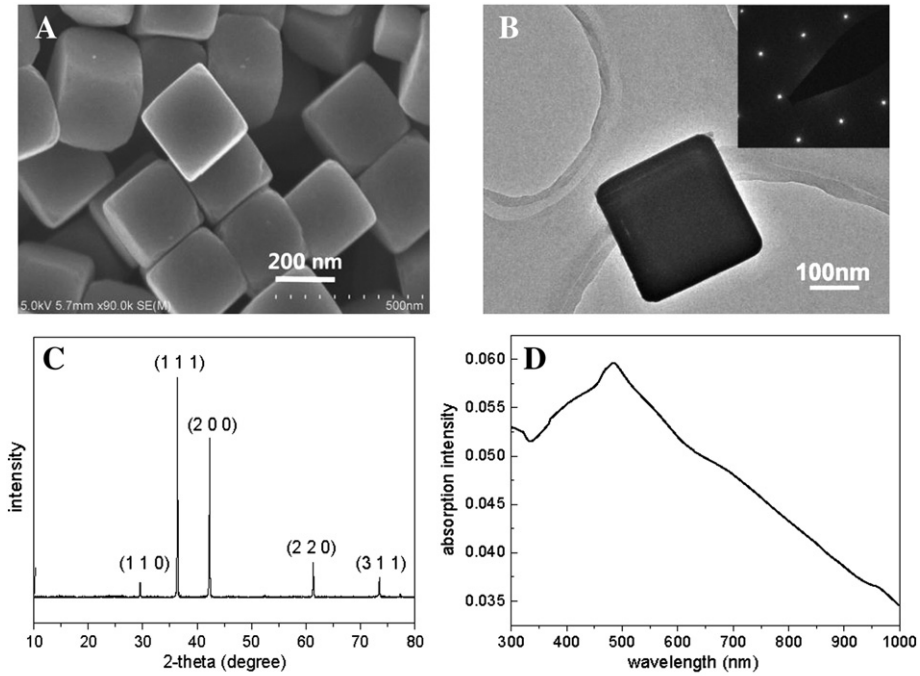


**Fig. 2.** (A) SEM images of $Cu_2O$ nanocubes synthesized via a typical procedure described in Section 2. (B) TEM images of $Cu_2O$ nanocubes synthesized in a typical procedure. (C) XRD pattern as-prepared samples obtained in typical experimental condition. (D) UV–visible spectrum recorded from the solution of cuprous oxide nanocubes dispersed in deionized water at room temperature.

reactant concentration, amount of surfactant, and stirring rates. In order to elucidate the effect of experimental parameter on the morphology of $Cu_2O$ nanocrystals, we carried out multi-group experiments. In each group of experiment, we only change one parameter and other parameters are kept as same as that of typical synthesis parameters in Section 2. It can be seen from Fig. 3 that the average particle size could be changed significantly by adjust the amount of surfactant and stirring rate. In Fig. 3, the morphology of particle also could be controlled from truncated cube to octahedron according to changing (111)/(100) surface area ratio.

Fig. 5 shows the $Cu_2O$ nanoparticles synthesized in our experiments. Fig. 5 A1–A4 reveals the morphologies of $Cu_2O$ nanoparticles synthesized at different amounts of surfactant. Without surfactant, only irregular nanoparticles are observed. With the help of surfactant, regular truncated nanocubes were formed. When the amount of surfactant increased from 0.18 mmol to 0.45 mmol, the average particle size changed from 100 nm to 500 nm. The presence of PVP seems beneficial to the growth of $Cu_2O$ nanocubes.

Temperature is a key factor in preparing uniform cubic $Cu_2O$ particles. Fig. 5 B1–B4 shows the SEM images of $Cu_2O$ nanocubes prepared at 30 °C, 40 °C, 50 °C and 90 °C, respectively. The morphology of particle changes from truncated cube to perfect cube with temperature arising from 30 °C to 50 °C, particles in three samples have smooth surface and particle size is uniform. Nanocubes prepared at 90 °C are corroded seriously and display uneven surfaces. With the rising of synthesis temperature, the average edge length of nanocubes exhibits a peak (500 nm) at 50 °C.

The concentration of reactant is another key factor that influences the morphology of $Cu_2O$ nanoparticles. According to our observation, at different copper acetate concentration, the most particles are truncated cube, and particle size varies from 100 nm to 1700 nm with the increase of copper acetate concentration. On the contrary, the amount of reducing agent has a great influence on morphology of productions. Fig. 5 C1–C4 are SEM image of $Cu_2O$ nanocubes prepared at 0.25, 0.5, 0.75 and 1 mmol of ascorbic acid respectively. When the amount of reducing agent was less than 0.25 mmol, the product mainly comprises of acicular $Cu(OH)_2$ nanowire. When the amount of reducing agent reaches 0.75 mmol, truncated cuprous oxide nanocubes with the average diameter about 120 nm are obtained (Fig. 3C). The shape of cuprous oxide particle changes to octahedron having rough surface with an increase in the amount of reducing agent to 1 mmol (Fig. 5 C4). When the amount of reducing agent was further increased to 1.25 mmol, there is no precipitation in solution after reaction.

An interesting finding in our experiments is that the morphology of nanoparticles was very sensitive to the stirring rate. Small adjusting of stirring rate will result in great changes of particle morphology. Fig. 5 D1–D4 indicated the SEM image of $Cu_2O$ nanoparticles synthesized at 4 r/s, 4.5 r/s, 5 r/s, 5.5 r/s of stirring rate respectively. The shape of nanoparticles changes from cube to truncated cube and then to spheres. At the same time, the average particle size decreases from 750 nm to 150 nm with the increase of stirring rate.

## 4. Discussion

### 4.1. Mechanism of $Cu_2O$ precipitation and crystal growth

We speculate that $Cu_2O$ tends to form nanocubes due to orientational crystallization mechanism. Cupric acetate could be dissolved in water and forms a uniform ionic solution. When the NaOH is added in the solution, the $Cu^{2+}$ reacts with $OH^-$ and forms blue insoluble $Cu(OH)_2$ precipitate. While $Cu(OH)_2$ suspension reacts with ascorbic acid, $Cu(OH)_2$ will be reduced into reddish $Cu_2O$ nanoparticles. It can be understood that the formation process of $Cu_2O$ nanoparticle composes the following three consecutive reactions:

$$Cu^{2+} + 2OH^- \rightarrow Cu(OH)_2\downarrow \quad (1)$$

$$Cu(OH)_2 + C_6H_8O_6 \rightarrow Cu^{2+} + 2H_2O + C_6H_6O_6^{2-} \quad (2)$$

$$2Cu^{2+} + C_6H_6O_6^{2-} + H_2O \rightarrow Cu_2O + C_6H_6O_6 + 2H^+ \quad (3)$$

The $Cu_2O$ tend to aggregate and to reduce their total surface energy after they precipitate from the solutions. When subsequent $Cu_2O$

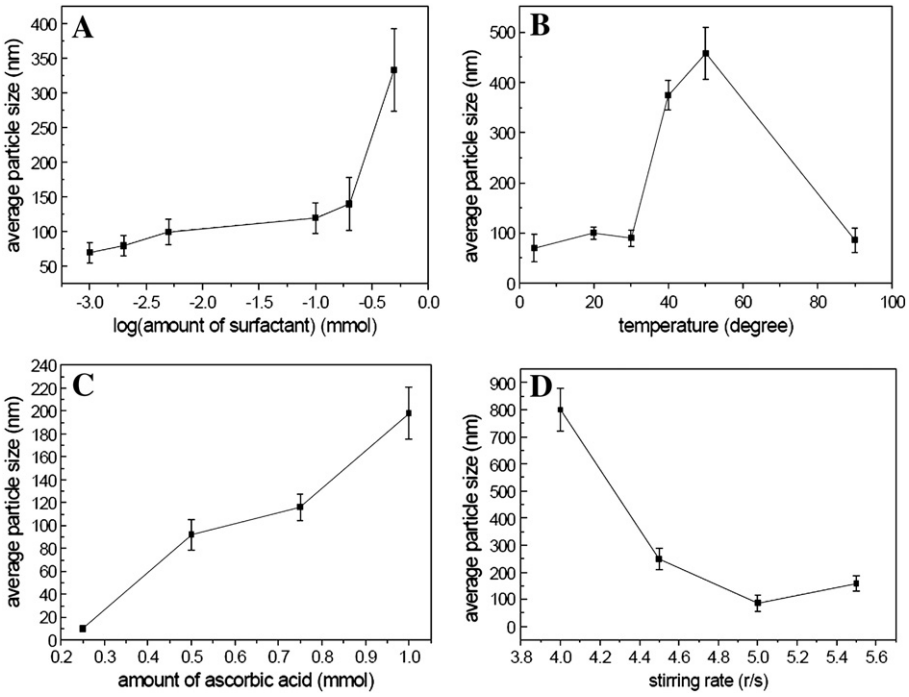


**Fig. 3.** Influence of preparing conditions on the size of $Cu_2O$ nanoparticles. (A) The average particle size as a function of surfactant amount. (B) The average particle size as a function of reaction temperature. (C) The average particle size as a function of the amount of ascorbic acid. (D) The average particle size as a function of stirring rate.

monomers precipitate from the solution, they tend to aggregate on the existing $Cu_2O$ seeds and grow up. In the absence of a hard template, low-dimensional structures are governed by thermodynamic (e.g., temperature, reduction potential) and kinetic (e.g., reactant concentration, diffusion, solubility, reaction rate) parameters. Fig. 6 schematic illustrates the morphology evolution of cuprous oxide nanoparticles at different synthetic conditions.

### 4.2. Influence of synthesis conditions on morphology

#### 4.2.1. Effects of surfactant on $Cu_2O$ morphology

It is reported that PVP has the selective adsorption properties to specific crystal planes, and could be used to kinetically control the growth of single-crystalline nanocubes [21]. We also find that surfactant plays an important role on morphology and average size of nanocrystals. When surfactant was added into the solution, the active molecule of surfactant was adsorbed on specific crystal plane of $Cu_2O$ nanocrystals because the adsorption energy of surfactant on different crystal plane was significantly different. Different type and different amount of surfactant not only affected interaction between crystal phase and solution phase, but also played a decisive role in determining the shape of crystal and the growth habit of the various crystal planes. The crystal planes with fast growth rate gradually disappeared and the crystal plane with slow growth was preserved finally. The selective adsorption of surfactant on the crystal surface promoted the difference of growth rate on different crystal plane and therefore accelerated the growth of particles, resulting in the formation of nanoparticles with certain morphology. Therefore, the mount of polymeric surfactant, in fact, generally a certain amount of surfactant will produce significant impact on size and morphology. If we do not add any surfactant, the growth of cuprous oxide will show the absence of any regularity. Without PVP surfactant, no nanocrystals will be obtained in our experiment (Fig. 5 A1). The structure of products is polycrystalline cluster, which indicates $Cu_2O$ nanoparticles aggregate in a disorderly manner. When PVP was added into the solution, monodispersed colloidal solutions of $Cu_2O$ nanocrystals with regular polyhedral shapes and bound entirely by {100} and {111} facets of the fcc crystal lattice are obtained (Fig. 5 A2–A4). It is observed that the $Cu_2O$ nanocubes with larger particle size are obtained at high PVP concentration, when the amount of PVP changes from 0 to 0.018 mmol, particle size increases from 100 to 700 nm (Fig. 5A). The results indicate that the existence of PVP promote the growth of $Cu_2O$ nanocube. The reason for the increment of particle size with amount of surfactant increasing was as follows. The concentration of surfactant was increased by the amount added increasing. According to the theory on crystal growth kinetics and feature of polymer surfactant [22], increasing of surfactant concentration leads to increasing of viscosity in solution. Viscosity increasing makes diffusion and migration of ions in solution become more difficult. On the other hand, increasing of surfactant also makes nucleation become more difficult. Consequently, the activation energy which refers to an ion to jump from the liquid phase on crystal nucleus and critical nucleation energy were both increased. On the basis of theory of crystal growth [23], the nucleation rate of nanocrystals was decreased and the growth rate of nanocrystals was relatively increased. A slow nucleation rate and a relatively fast growth rate lead a crystal with larger average size. In the process of crystal growth, the surfactant can effectively reduce the grain surface energy, which can effectively reduce the grain adhesion, in addition to promoting the formation of regular morphology. On the other hand, when the concentration of surfactant was too high, the prepared nanoparticle easily aggregated due to polymer surfactant adhesion.

#### 4.2.2. Effects of temperature on $Cu_2O$ morphology

As an important thermodynamic parameter, temperature exhibits a significant influence on the morphology of nanocrystals. At the room temperature, by the help of surfactants (it is believed that the selective interaction between PVP and {100} planes of $Cu_2O$ could greatly reduce the growth rate along the <100> direction [24]), truncated $Cu_2O$ nanocubes are synthesized. From energy point of view, this structure is stable. Because the corners of nanocube have larger specific surface area, the corners of nanocubes are corroded and truncated along the {111} planes. With the rising of synthesis temperature, diffusion and migration rate of the ions and monomers increase, the nanocubes grow fast along the <111> directions (Fig. 6 B1–B4). Morphology of product changed gradually from truncated nanocube to nanocube (Fig. 5 B1–B3). Therefore,

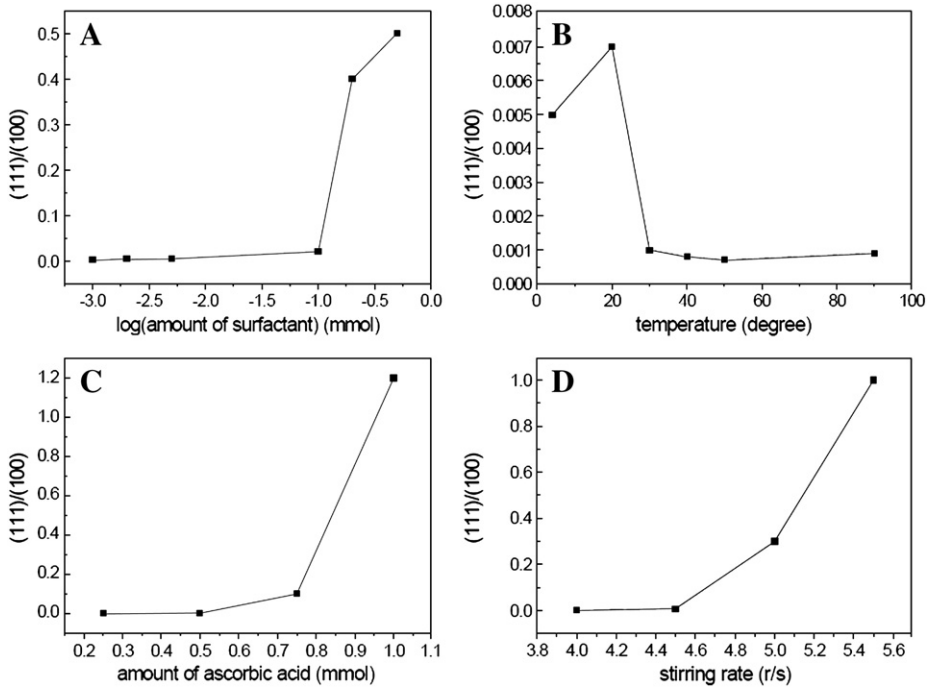


**Fig. 4.** Effect of preparing conditions on the morphologies of $Cu_2O$ nanoparticles. (A) (111)/(100) surface area ratio vs. amount of surfactant. (B) (111)/(100) surface area ratio vs. temperature. (C) (111)/(100) surface area ratio vs. amount of ascorbic acid. (D) (111)/(100) surface area ratio vs. stirring rate.

(111)/(100) surface area ratio was reduced rapidly with temperature rising (Fig. 4B). At the same time, particle size increased significantly (Fig. 3B). However, too high temperature will result in heavy erosion of cube surface. This will lead to imperfect cube particles with severe adhesion.

*4.2.3. Effects of reducing agent on $Cu_2O$ morphology*

Ascorbic acid is a mild reducing agent; it could reduce $Cu(OH)_2$ and form $Cu_2O$ nanocube. The redox chemical process for the formation of the $Cu_2O$ phase in solution was proposed in the above reaction Eqs. (2)–(3). Step (2) is actually the process of acid–base neutralization process and reaction rate was faster. Step (3) is redox reaction. Typically crystal nucleation in solution requires $Cu_2O$ monomer supersaturation. Without ascorbic acid, the concentration of $Cu^{2+}$ is too low to obtain $Cu_2O$ nucleation in solution (Fig. 5 C1). If ascorbic acid was added into solution, $Cu^{2+}$ was ionized out continuously, according to the reaction Eq. (2). When the concentration of $Cu^{2+}$ reached a certain degree, $Cu^{2+}$ begun to react with the ascorbic acid and began to a small amounts of cuprous oxide particles was produced (Fig. 5 C2). When the amount of ascorbic acid was further increased, $Cu(OH)_2$ was completely consumed. There was a large amount of $Cu_2O$ nanocubes generated. At the same time, ascorbic acid behaves as a vinylogous carboxylic acid. Excessive amount of ascorbic acid will corrode the $Cu_2O$ nanocubes via a dismutation reaction. $H^+$ will etch area with relatively high surface energy firstly, such as corners of nanocube, to form nanocubes with the rough surface (Fig. 5 C3). Since the {100} planes of nanocubes are selective adsorbed by surfactant PVP, {111} planes become candidates for selective corrosion. The direction of crystal growth was also along the <111> direction (Fig. 4C) and the average size became larger (Fig. 3C). With the increase of the amount of ascorbic acid, the morphology of $Cu_2O$ nanocubes varies from truncated cube to cuboctahedra and further becomes octahedron (Fig. 6 C2–C4).

Further increasing the amount of ascorbic acid will cause the complete corrosion of $Cu_2O$ nanoparticles, and the suspension turns to be a transparent solution again. No solid precipitation was obtained after centrifugation. This finding is of great value, because previous report [25–27] indicates that {111} planes of $Cu_2O$ particles have high catalytic activity.

*4.2.4. Effects of stirring rate on $Cu_2O$ morphology*

In the nucleation process, supersaturation of $Cu_2O$ provides a thermodynamic driving force. Dynamics force also needs to be satisfied for particle selective grow up. In addition to the thermodynamic and kinetic parameters, the shape of $Cu_2O$ nanoparticle is very sensitive to the stirring rate. In fact, the rapid stirring rate actually hinders the combination between different particles and prevented the crystal from growth. Furthermore, the high stirring rate will enhance

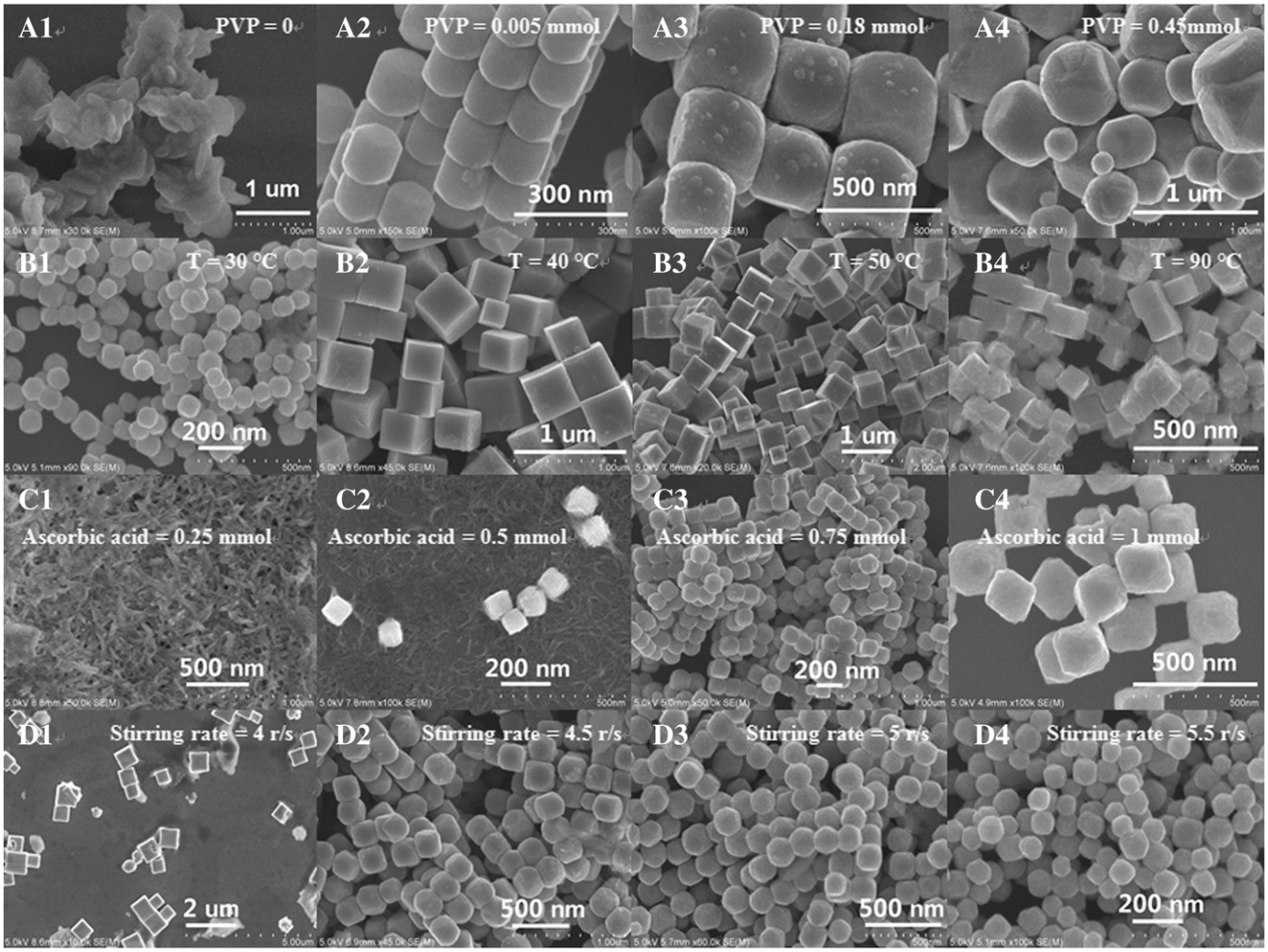


**Fig. 5.** SEM images of $Cu_2O$ nanoparticles fabricated at different synthetic conditions. From images A to D, we change the synthesis conditions, such as surfactant volume fraction, temperature, reducing agent concentration and stirring rate, respectively. From A1 to A4, the PVP changed from 0 to 0.45 mmol. From B1 to B4 the temperature varied from 30 °C to 90 °C. From C1 to C4, the amount of ascorbic acid increased from 0. 25 mmol to 1 mmol. From D1 to D4, stirring rate increased from 4 r/s to 5.5 r/s.

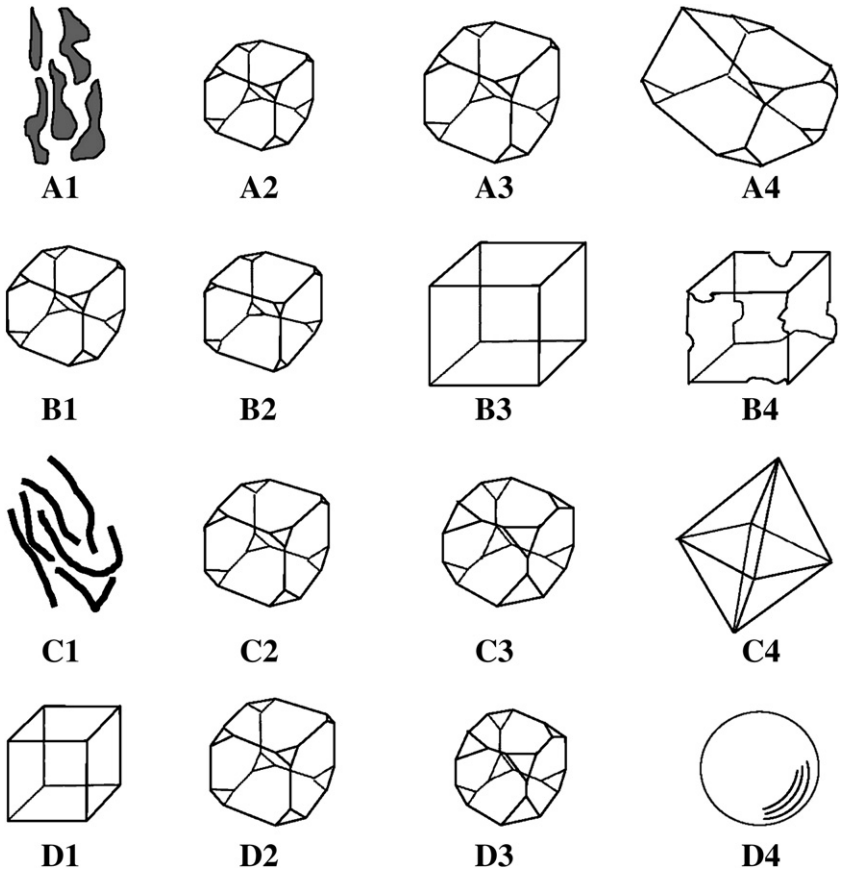


**Fig. 6.** Schematic illustration of the morphology evolution of cuprous oxide nanoparticles. From rows A to D indicate the morphology evolution by the change of surfactant amount, temperature, amount of reducing agent and stirring rate, respectively.

the probability and energy of collision between particles and vessel wall (or between themselves). Mechanical wear and erosion make the corners and edges of $Cu_2O$ nanocubes disappear gradually (Fig. 6 D1–D4). When the stirring rate is 4 r/s, perfect cuprous oxide nanocubes with average edge length of 800 nm are synthesized (Fig. 5 D1). While the stirring rate increases to 5 r/s, truncated cubes with the average diameter of 250 nm are formed in solution. When stirring rate reaches 6 r/s, only 150 nm diameter of nanospheres can be found in the product. The average size of nanoparticle was declined with the stirring rate increasing (Fig. 3D).

Moreover, at higher stirring rate, more oxygen can be dissolved in water. Ascorbic acid in solution is very sensitive to the oxygen concentration in water; higher oxygen concentration will make ascorbic acid easy to be oxidized and lose reducibility and acidity. So there is no $Cu_2O$ particles obtained when the stirring rate is higher than 6 r/s.

## 5. Conclusion

In this paper, cuprous oxide nanoparticles with different morphologies have been successfully synthesized by a wet-chemical approach in aqueous solution. XRD and TEM results indicate that the cuprous oxide particles are truncated nanocubes bounded by {100} and {111} facets. By the adjusting of synthesis conditions, $Cu_2O$ nanocubes, truncated nanocubes, cuboctahedra, nanosphere, and octahedra are synthesized. Growth mechanism of these nanoparticles is interpreted as the combination effect of selective growth, selective corrosion and mechanical erosion of $Cu_2O$ nanocrystals. These $Cu_2O$ nanoparticles should find applications in a variety of areas such as photonics, catalysis, and sensing. This work and previous demonstrations from other groups [28–32] indicate that $Cu_2O$ nanoparticles with well-controlled shapes, sizes, and structures can be obtained by the optimization of thermodynamic and kinetic parameters.

## Acknowledgment

This work was supported by the National Basic Research Program of China (No. 2010CB832905), and the Key Scientific and Technological Project of the Ministry of Education of China (No. 108124).

## References

[1] I. Grozdanov, Materials Letters 19 (1994) 281.
[2] M.Y. Shen, T. Yokouchi, S. Koyama, T. Goto, Physical Review B 56 (1997) 13066.
[3] R.M. Habiger, A. Compaan, Solid State Communications 18 (1976) 1532.
[4] B. Lefez, M. Lenglet, Chemical Physics Letters 179 (1991) 223.
[5] W. Shi, K. Lim, X. Liu, Journal of Applied Physics 81 (1997) 2822.
[6] D. Snoke, Science 273 (1996) 1351.
[7] R.N. Briskman, Solar Energy Materials and Solar Cells 27 (1992) 361.
[8] X. Li, H. Gao, C.J. Murphy, L. Gou, Nano Letters 4 (2004) 1903.
[9] R. Liu, E.A. Kulp, F. Oba, E.W. Bohannan, F. Ernst, J.A. Switzer, Chemistry of Materials C 17 (2005) 725.
[10] M. Hara, T. Kondo, M. Komoda, S. Ikeda, K. Shinohara, A. Tanaka, J.N. Kondo, K. Domen, Chemical Communications 3 (1998) 357.
[11] Su-Kyung Lee, Young-Hwan Yoon, Heon Kang, Electrochemistry Communications 11 (2009) 676.
[12] Yongsong Luo, Youchao Tu, Qinfeng Ren, Xiaojun Dai, Lanlan Xing, Jialin Li, Journal of Solid State Chemistry 182 (2009) 182.
[13] Zhenghua Wang, Hui Wang, Lingling Wang, Ling Pan, Journal of Physics and Chemistry of Solids 70 (2009) 719.
[14] Xu Zhang, Yi Xie, Fen Xu, Xiaohui Liu, Di Xu, Inorganic Chemistry Communications 6 (2003) 1390.
[15] Haolan Xu, Wenzhong Wang, Wei Zhu, Microporous and Mesoporous Materials 95 (2006) 321.
[16] Lei Huang, Feng Peng, Hao Yu, Hongjuan Wang, Materials Research Bulletin 43 (2008) 3407.
[17] Y. Yu, F.P. Du, J.C. Yu, Y.Y. Zhuang, P.K. Wong, Journal of Solid State Chemistry 177 (2004) 4640.

[18] Ho Sun Shin, Jae Yong Song, Jin Yu, Materials Letters 63 (2009) 397.
[19] L. Gou, C.J. Murphy, Journal of Materials Chemistry 14 (2004) 735.
[20] L. Gou, C.J. Murphy, Nano Letters 3 (2003) 231.
[21] H. Xu, W. Wang, W. Zhu, The Journal of Physical Chemistry. B 110 (2006) 13829.
[22] Marcio Luis Ferreira Nascimento, Eduardo Bellini Ferreira, Edgar Dutra Zanotto, The Journal of Chemical Physics 121 (2004) 8924.
[23] Claudio L. De Castro, Brian S. Mitchell, Materials Science and Engineering A 396 (2005) 124.
[24] E. Ko, J. Choi, K. Okamoto, Y. Tak, J. Lee, Chemphyschem 7 (2006) 1505.
[25] Y.H. Lee, I.C. Leu, C.L. Liao, S.T. Chang, M.T. Wu, J.H. Yen, K.Z. Fung, Electrochemical and Solid-State Letters 9 (2006) A207.
[26] I. Lisiecki, M.P. Piled, The Journal of Physical Chemistry 99 (1995) 5077.
[27] Wei-Tai Wu, Yusong Wang, Lei Shi, Wenmin Pang, Qingren Zhu, Guoyong Xu, Fei Lu, The Journal of Physical Chemistry B 110 (2006) 14702.
[28] M. Yin, C. Wu, Y. Lou, C. Burda, J.T. Koberstein, Y. Zhu, S. O'Brien, Journal of the American Chemical Society 127 (2005) 9506.
[29] R.J. Darey, B. Milisarljeric, J.R. Bourne, The Journal of Physical Chemistry 92 (1988) 2032.
[30] Yugang Sun, Younan Xia, Science 298 (2002) 2176.
[31] Jin-Yi Ho, Michael H. Huang, The Journal of Physical Chemistry 113 (2009) 14159.
[32] Chun-Hong Kuo, Michael H. Huang, The Journal of Physical Chemistry 112 (2008) 18355.